ADVANCED TOKAMAK PHYSICS IN DIII–D

by

C.C. PETTY, T.C. LUCE, P.A. POLITZER, M.R. WADE, S.L. ALLEN, M.E. AUSTIN, B. BRAY,
K.H. BURRELL, T.A. CASPER, M.S. CHU, J.R. FERRON, E.D. FREDRICKSON, A.M. GAROFALO,
P. GOHIL, I. GORELOV, C.M. GREENFIELD, W.W. HEIDBRINK, C.-L. HSIEH, A.W. HYATT,
R. JAYAKUMAR, L.C. JOHNSON, J.E. KINSEY, R.J. LA HAYE, L.L. LAO, C.J. LASNIER,
E.A. LAZARUS, A.W. LEONARD, Y.R. LIN-LIU, J. LOHR, M.A. MAHDAVI, M.A. MAKOWSKI,
G.R. McKEE, M. MURAKAMI, G.A. NAVRATIL, M. OKABAYASHI, T.W. PETRIE, R.I. PINSKER,
R. PRATER, C.L. RETTIG, T.L. RHODES, B.W. RICE, J.T. SCOVILLE, G.M. STAEBLER, E.J. STRAIT,
T.S. TAYLOR, J.G. WATKINS, W.P. WEST, N.S. WOLF, and K.-L. WONG

JULY 2000

DISCLAIMER

ADVANCED TOKAMAK PHYSICS IN DIII–D

by

C.C. PETTY, T.C. LUCE, P.A. POLITZER, M.R. WADE,* S.L. ALLEN,[†] M.E. AUSTIN,[‡] B. BRAY,
K.H. BURRELL, T.A. CASPER,[†] M.S. CHU, J.R. FERRON, E.D. FREDRICKSON,[△] A.M. GAROFALO,[#]
P. GOHIL, I. GORELOV, C.M. GREENFIELD, W.W. HEIDBRINK,[◊] C.-L. HSIEH, A.W. HYATT,
R. JAYAKUMAR,[†] L.C. JOHNSON,[△] J.E. KINSEY,[∞] R.J. LA HAYE, L.L. LAO, C.J. LASNIER,[†]
E.A. LAZARUS,* A.W. LEONARD, Y.R. LIN-LIU, J. LOHR, M.A. MAHDAVI, M.A. MAKOWSKI,[†]
G.R. McKEE,[¶] M. MURAKAMI,* G.A. NAVRATIL,[#] M. OKABAYASHI,[△] T.W. PETRIE, R.I. PINSKER,
R. PRATER, C.L. RETTIG,[§] T.L. RHODES,[§] B.W. RICE,[†] J.T. SCOVILLE, G.M. STAEBLER, E.J. STRAIT,
T.S. TAYLOR, J.G. WATKINS,[□] W.P. WEST, N.S. WOLF,[†] and K.-L. WONG[△]

*Oak Ridge National Laboratory, Oak Ridge, Tennessee.
[†]Lawrence Livermore National Laboratory, Livermore, Califoronia.
[‡]University of Texas, Austin, Texas.
[△]Princeton Plasma Physics Laboratory, Princeton, New Jersey.
[#]Columbia University, New York, New York.
[◊]University of California, Irvine, California.
[∞]Lehigh University, Bethlehem, Pennsylvania.
[¶]University of Wisconsin, Madison, Wisconsin.
[§]University of California, Los Angeles, California.
[□]Sandia National Laboratories, Albuquerque, New Mexico.

ABSTRACT

Advanced tokamaks seek to achieve a high bootstrap current fraction without sacrificing fusion power density or fusion gain. Good progress has been made towards the DIII–D research goal of demonstrating a high-β advanced tokamak plasma in steady-state with a relaxed, fully non-inductive current profile and a bootstrap current fraction greater than 50%. The limiting factors for transport, stability, and current profile control in advanced operating modes are discussed in this paper.

1. INTRODUCTION

The tokamak has proved to be a remarkable plasma confinement device over the last four decades. The largest tokamaks have achieved ion temperatures in excess of 40 keV [1] and fusion powers in excess of 16 MW using a mixture of deuterium and tritium ions [2], and even small tokamaks built by university students have achieved plasma temperatures of 0.1 keV [3]. A "conventional" tokamak that operates at high plasma current with an ELMing (edge localized mode) H–mode edge is an excellent candidate for a burning plasma experiment in the near future [4]. However, an inherent drawback of the tokamak as a fusion power plant is the large plasma current that must be sustained to gain the benefits (such as lessening material fatigue problems) that derive from steady-state operation of any magnetic confinement fusion reactor. For a tokamak, steady-state operation implies a bootstrap current fraction of 70% or higher, otherwise the power needed for non-inductive current drive would be unaffordable.

A major focus of the DIII–D program is to develop the scientific basis for advanced modes of operation that can enhance the commercial attractiveness of the tokamak as an energy producing system. Features that improve the attractiveness of the tokamak as a fusion reactor include: high fusion power density which requires high β (the ratio of the plasma pressure to the magnetic field pressure), high fusion gain which entails high $\beta\tau$ (τ is the energy confinement time), and steady-state operation with low recirculating power which demands high f_{bs} (the bootstrap current fraction). The product $\beta\tau$ is a critical parameter because it is proportional to the fusion power divided by the heating power required to sustain the plasma. The bootstrap current fraction increases with safety factor (q) like $f_{bs} \propto q^2\beta$ [5]; thus, high β and a high edge safety factor in the range of $q_{95} \sim 5$ are needed in advanced tokamak modes. However, increasing q without decreasing β also requires an improvement in the plasma stability limit because the normalized beta (β_N) is proportional to $\beta_N \propto q\beta$. Finally, since the energy confinement time is observed to have a nearly linear dependence on the plasma current, the confinement factor ($H_{89} = \tau/\tau_{89}$, where τ_{89} is a confinement scaling relation for L–mode plasmas [6]) will need to increase like $H_{89} \propto q$ in advanced tokamak modes to achieve a similar fusion gain ($\beta\tau$) as in the conventional tokamak mode. In this paper, the values of τ and H_{89} are corrected for the time varying stored energy and heating power. The product $\beta_N H_{89}$ is a good figure of merit for determining how well an advanced tokamak mode does in increasing the bootstrap current fraction without sacrificing fusion power density or fusion gain.

2. COMPARISON OF CONVENTIONAL AND ADVANCED OPERATING MODES

A near-term goal of the DIII–D research program is the development and demonstration of high-β advanced tokamak plasmas with $f_{bs} > 0.5$ and plasma profiles that are close to those anticipated for steady-state operation. Significant progress has recently been made towards this goal, as shown in Fig. 1 for a discharge with a neutral beam injection (NBI) heating power of $P_{nb} = 11$ MW, toroidal magnetic field strength of $B_T = 1.6$ T, plasma current of $I_p = 1.2$ MA, major radius of $R = 1.66$ m, minor radius of $a = 0.60$ m, elongation of $\kappa = 2.0$, and triangularity of $\delta = 0.8$. The plasma geometry and safety factor profile ($q_{95} = 5.4$) are chosen to maximize stability to ballooning modes and to low-n kink modes, as discussed in Section 4, so that the sustained value of β_N is increased over the previous best result in DIII–D [7]. The normalized beta, $\beta_N = \beta/(I_p/aB_T) = 3.7$, exceeds the ideal limit for a plasma without a conducting wall ($\approx 4\ \ell_i$, where ℓ_i is the internal inductance) [8] by about 15% during the high performance phase, although this value of β_N is still well below the ideal limit for a plasma with a close-fitting conducting wall. The advanced tokamak discharge in Fig. 1 exhibits sustained high performance with $\beta_N H_{89} > 9$ for 2 s, which is 16 energy confinement times or about one current profile relaxation time.

The main difference between the conventional and advanced operating modes is not in the tokamak fusion performance, but rather in the bootstrap current fraction. This is shown in Fig. 2, where the time histories of two plasmas with different safety factors are compared. Both plasmas have the same value of B_T and the same plasma shape as the discharge in Fig. 1, and both plasmas
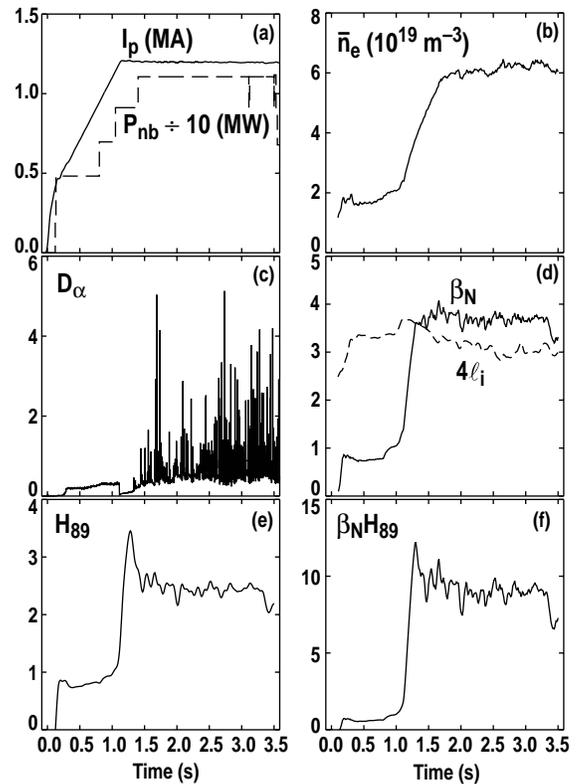
Fig. 1. DIII–D discharge 98977 parameters *vs.* time. (a) Plasma current and NBI power, (b) line-averaged density, (c) D_α signal from divertor region, (d) normalized beta compared to 4× the internal inductance, and (e) confinement time normalized to ITER-89P scaling, and (f) combined figure of merit for advanced tokamaks.

have an ELMing H–mode edge. The higher I_p case is a conventional tokamak discharge with q_{95} = 3.1 and infrequent giant ELMs triggered by sawtooth crashes. Because of the relatively high density, up to 2/3 of the density limit, the electron and ion temperatures are equilibrated. The normalized beta saturates at β_N = 2.7 after the onset of a rotating m/n = 3/2 mode starting at 2.2 s that has the characteristics of a neoclassically destabilized tearing mode (NTM). Since the normalized current is large in the conventional mode, I_p/aB_T = 2.0 MA/mT, a high value of beta is reached, β = 5.3%. The confinement factor is H_{89} = 1.8 for this discharge which is ≈10% lower than expected for H–mode confinement, probably due to the effects of the tearing mode [9,10]. The conventional tokamak discharge terminates when a m/n = 2/1 rotating tearing mode is destabilized by a sawtooth crash at 3.0 s, leading to a disruption. Future fusion reactors may be immune to NTMs because the inherently larger value of the magnetic Reynold's number may decouple the q = 3/2 surface from the q = 1 sawtooth so that the seed island will be too small to sufficiently disturb the metastable plasma state [11].

Fig. 2. Comparison of advanced tokamak discharge 98549 (solid lines) and conventional tokamak discharge 100256 (dashed lines). (a) Plasma current, (b) NBI power, (c) line-averaged density, (d) bootstrap current fraction, (e) beta, (f) normalized beta, (g) confinement time, and (h) confinement time normalized to ITER-89P scaling.

The lower I_p case in Fig. 2 is an advanced tokamak discharge with q_{95} = 5.5 and frequent ELMs. The density is about half that of the conventional tokamak mode, owing to the lower plasma current, resulting in a central ion temperature (T_i) that is twice the electron temperature (T_e). This hot ion mode of operation is common for advanced tokamak plasmas in DIII–D [12,13]. Figure 2 shows that beta for the advanced mode, β = 4.6%, is less than that for the conventional mode; however, the normalized beta is higher, β_N = 3.8, because of the 40% lower plasma current. The smaller plasma current also results in an energy confinement time that is 14% lower for the advanced mode than the conventional mode despite the higher confinement factor, H_{89} = 2.7. Resistive wall modes (RWM) play a role in limiting β during the quasi-stationary portion of this discharge, as

discussed in Section 4. The sudden growth in the RWM at 3.2 s leads to a drop in β that destabilizes a $m/n = 2/1$ tearing mode, resulting in a severe degradation in confinement. Figure 2 shows that while $\beta\tau$ for the conventional mode can be superior to that of the advanced mode, the latter achieves its central objective by increasing the bootstrap current fraction to $f_{bs} = 0.58$ (compared to $f_{bs} = 0.24$). The higher value of f_{bs} is related to the increase in $\beta_N H_{89}$ from 4.9 for the conventional operating mode to 10.0 for the advanced mode.

3. TRANSPORT IN ADVANCED TOKAMAKS

The heat transport for the advanced tokamak mode is similar to that of the conventional mode despite the higher safety factor (lower plasma current). This is shown in Fig. 3, where the thermal diffusivities determined by the TRANSP transport code [14] are plotted for the advanced and conventional tokamak discharges of Fig. 2 during the quasi-stationary H–mode phases. Only the effective (one fluid) diffusivity (χ_{eff}) is shown for the conventional mode because it is difficult to separate the electron and ion fluids owing to the high density, whereas the separate ion (χ_i) and electron (χ_e) diffusivities are given for the advanced mode. The ion diffusivity for the advanced tokamak case is 2–3 times the neoclassical level [15], indicating that anomalous transport from plasma turbulence is present. The increase in the neoclassical diffusivity above the measured levels near the plasma center is not meaningful since the theory breaks down in that region.

The enhanced confinement in advanced tokamak plasmas is likely due to the *E×B* shear acting to reduce the overall level of turbulent transport as well as the stabilizing effects of the fast beam ions and $T_i > T_e$. Figure 4 shows a simulation of the ion and electron temperature profiles using the gyro-Landau-fluid GLF23 drift wave transport model [16] in the MLT code [17]. In the simulation, the measured density and toroidal velocity profiles are utilized, the poloidal velocity profile (which gives only a small contribution to
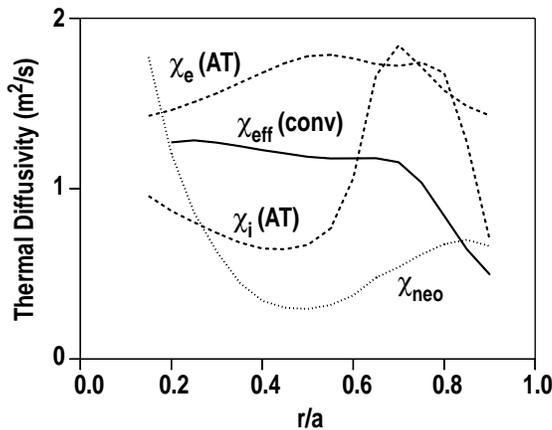
Fig. 3.   Thermal diffusivities as a function of normalized radius for the conventional tokamak plasma at 2.45 s (solid line) and the advanced tokamak plasma at 2.7 s (dashed lines) of Fig. 2. The neoclassical ion thermal diffusivity for the advanced mode is also shown (dotted line).
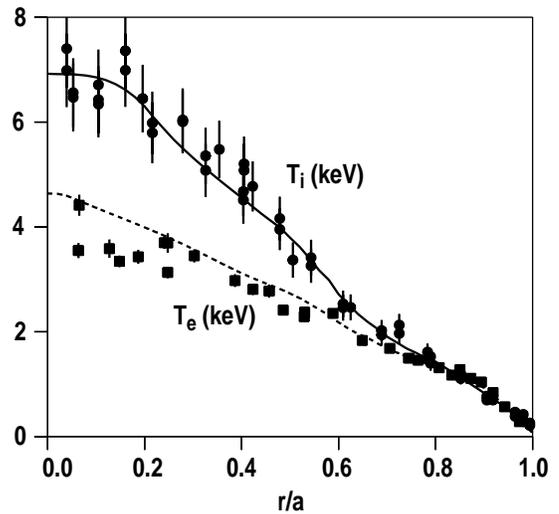
Fig. 4.   Comparison between the measured T_i (circles) and T_e (squares) profiles and the predicted profiles from the GLF23 transport model (solid and dashed lines) for the advanced tokamak discharge of Fig. 2 at 2.7 s.

the *E×B* shear) is calculated from neoclassical theory, and the T_i and T_e profiles are calculated using the radial heat fluxes obtained from a power balance analysis. The GLF23 transport model is in good agreement with the measured T_i profile but it overestimates T_e. The ion temperature gradient (ITG) mode [18,19] is the dominant instability found in the model. Since *E×B* shear reduces transport by connecting unstable modes to stable modes [20], the saturated fluctuation intensity in the GLF23 transport model is taken to be proportional to the difference between the maximum growth rate from linear theory and the *E×B* shear rate [21], as shown in Fig. 5. While the *E×B* shear is acting to reduce the overall

Fig. 5. Radial dependence of the maximum growth rate (solid line) and E×B shear rate (dashed line) calculated by the GLF23 transport model for the case shown in Fig. 4. The rates are normalized by $\sqrt{T_e/m_i}\,/a$.

level of transport, the turbulence is not eliminated in the simulation. Instead, the ion temperature profile lies near the instability threshold where both the maximum growth rate and the *E×B* shear rate are relatively small (the "first stability'" point near the zero of the net growth rate [22]). The maximum growth rate and *E×B* shear rate in Fig. 5 are strongly correlated across the plasma radius because the GLF23 simulation uses a strong critical gradient model with a large incremental diffusivity for the transport driven by the ITG mode. The hot ion mode and the dilution of the thermal ions by fast beam ions are also important stabilizing influences in the core that result in reduced transport for advanced tokamak discharges [22,23].

Impurity seeding may be one method for further improving the confinement in advanced modes without deleterious effects. In general, narrow internal transport barriers (ITBs) are detrimental to advanced tokamaks because of the reduced stability limits associated with the large pressure gradient and the poor alignment between the bootstrap current profile and the total current profile. The reduced β limit observed experimentally in plasmas with ITBs is consistent with the predicted dependence on the pressure profile peakness based on ideal $n = 1$ stability theory [24]. Thus, any method used to reduce the transport in advanced tokamaks should preferably do so across the entire radial profile. Experiments with neon seeding of L–mode plasmas in DIII–D have demonstrated a global reduction in the ion and electron heat transport, resulting in broadened temperature profiles with increased central values while causing only a small dilution of the core fuel ions [25,26]. Gyrokinetic simulations indicate that the linear growth rates and nonlinear saturated turbulence levels are reduced by the effect of impurity ions on the stability of ITG
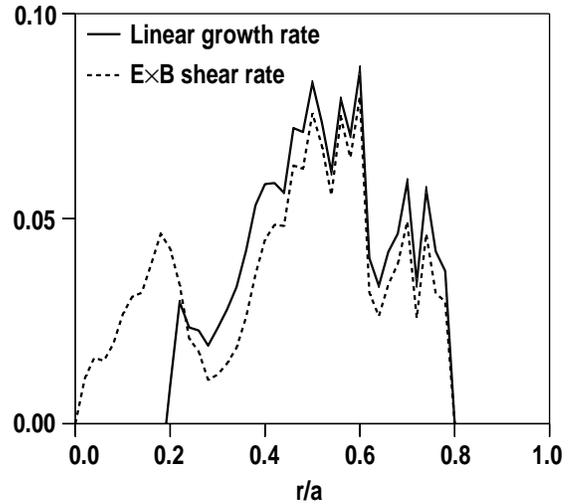
modes as a result of one of several mechanisms: dilution of the main fuel ions, direct mode stabilization by impurity ions, and temperature gradient changes resulting from enhanced localized radiation [26]. The reduction in the growth rates also acts synergistically with the $E \times B$ shear, owing to the larger toroidal velocity that results from a reduction in momentum transport, to further suppress the plasma turbulence. Impurity seeding of advanced modes may also help to establish a radiating mantle around the core of the plasma that would reduce the heat flux conducted to plasma facing surfaces.

4. STABILITY LIMITS IN ADVANCED TOKAMAKS

Stability plays a key role in advanced operating modes like the one shown in Fig. 1 since MHD phenomena limit the initial rise of the plasma energy after the H–mode transition, maintain a quasi-stationary state afterwards, and eventually cause the discharge to lose energy. The rapid β rise after the H–mode transition ends with the onset of high frequency MHD modes that are consistent with Alfvènic modes driven by fast ions [13]. This instability recurs in a bursting fashion throughout the discharge. However, RWMs are the most common β limiting phenomena during the quasi-stationary phase of the discharge; the safety factor profile has a minimum q value just above 1.5 with weak negative shear in the inner region that eliminates the $q = 3/2$ surface from the plasma and provides stability to ballooning modes while the outer region has strong positive shear that is correlated with improved NTM stability. The RWM is expected to appear when β_N exceeds the ideal no-wall stability limit. As shown in Fig. 6, a slowly rotating $n = 1$ mode comes and goes during the high β phase of the advanced tokamak discharge. The real frequency in the laboratory frame is below 100 Hz which is consistent with the resistive wall time rather than the plasma rotation rate. The RWM is predicted to be stabilized by sufficiently high plasma rotation, but the RWM itself can lead to slowing of rotation. Figure 6 shows that β drops as the RWM amplitude rises, which can lead to the RWM quenching and a recovery in β [27]. The high performance phase is often terminated when a RWM grows to large amplitudes instead of quenching owing to a large decrease in the plasma toroidal velocity [28].

Progress has been made recently in active feedback stabilization of the RWM [27,29], which may allow β_N to be raised closer to the ideal wall-stabilized limit in future advanced tokamak plasmas. The feedback coil set consists of six window frame coils located outside the vacuum vessel on the midplane. Saddle coil sensors monitoring the $n = 1$ helical flux leakage are also mounted outside of the vessel wall. Figure 7 shows a proof of principle experiment where feedback is applied in a negative central shear plasma. When β_N is near to the ideal stability limit without a wall, a
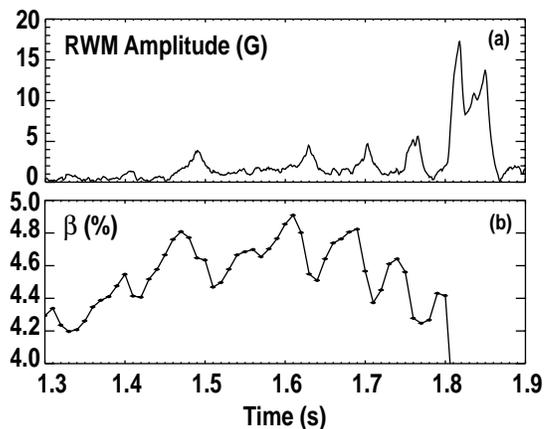
Fig. 6. Repeated appearance and quenching of the RWM in discharge 98526. (a) The $n = 1$ component of flux measured by three saddle loop pairs, and (b) beta.

RWM is gradually excited accompanied by a reduction in the plasma toroidal rotation. Without feedback, the mode grows rapidly before 1.4 s and a sudden drop in β and rotation is observed. When feedback is applied, Fig. 7 shows that the high β phase of the discharge is modestly extended by 0.2 s and the rate of rotational slowing is greatly reduced.
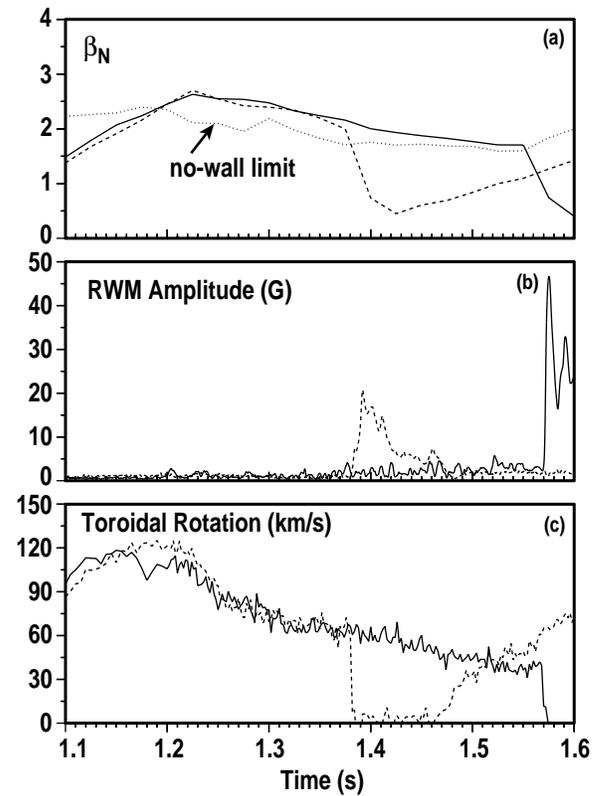
Fig. 7. Comparison of discharge 102731 with active feedback stabilization of RWM (solid line) and discharge 102728 without (dashed line). (a) Normalized beta compared to the ideal no-wall stability limit, (b) the $n = 1$ component of flux measured by three saddle loop pairs, and (c) plasma toroidal velocity at $r/a \approx 0.5$.

5. CURRENT PROFILE CONTROL

A key obstacle to extending the duration of advanced tokamak modes in DIII–D is the continual evolution of the current profile toward a less stable configuration. The initial current profile is formed using a combination of early NBI, ramping of the plasma current, and controlled H–mode transitions [30]. During the high performance H–mode phase, the minimum in q decreases and moves towards the plasma center, the edge current density increases, and the shear in the outer region is reduced. The rise in the edge current density increases the instability drive for RWMs, and the decrease in the shear aggravates the NTM instability. The cause of the current profile evolution can be seen in Fig. 8, where the measured components[31] of the total current profile (J_{tot}) during the high performance H–mode phase are plotted. The bootstrap current is >50% of the total current, with a profile (J_{bs}) that is flat across most of the plasma except near the edge where it peaks because of the H–mode pedestal. The neutral beams drive an additional ≈25% of the plasma current, with a profile (J_{nb}) peaked at the center. The residual inductive current density (J_{oh}) provides the remaining ≈25% of the total current and is peaked around $r/a \approx$ 0.5. To demonstrate quasi-stationary operation, it will be necessary to replace the inductive current with external current drive at the half radius.

In DIII–D, electron cyclotron current drive (ECCD) has been chosen to control and sustain the current profile in advanced tokamak plasmas because it has been shown to effectively drive localized current off-axis [32,33]. An example of the localization that is achievable with ECCD is shown in Fig. 9, which plots the change in the total current density ($\Delta J_{tot} \propto -\mu_0^{-1}$ $\partial B_z / \partial R$, where B_z is the vertical magnetic field strength measured by the motional Stark effect diagnostic [34]) during ECCD for two different resonance locations in

Fig. 8. Components of the current profile for the advanced tokamak plasma of Fig. 2 at 2.6 s.

MHD-quiescent L–mode plasmas. The width, location, and magnitude of the ECCD is in agreement with theoretical expectations including quasi-linear effects and current drive enhancement from the residual inductive electric field [35]. Current drive out to the half radius has been measured. To obtain the required non-inductive current from ECCD in

future advanced tokamak plasmas, the density in the H–mode phase will need to be reduced using controlled ELMs and the cryopump and baffle systems in DIII–D.
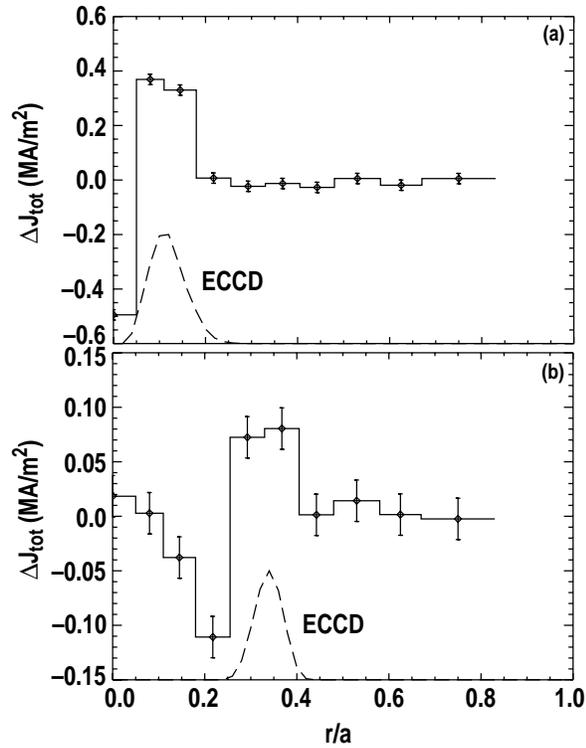
Fig. 9: Change in the measured total current density during off-axis ECCD for a resonance location of (a) *r/a* = 0.12, and (b) *r/a* = 0.34. The theoretical ECCD profiles are calculated using the torayGA code.

6. CONCLUSIONS

Good progress has been made towards the DIII–D research goal of demonstrating a high-β advanced tokamak plasma in steady-state with a relaxed, fully non-inductive current profile and $f_{bs} > 0.5$. A discharge with $\approx 75\%$ non-inductive current has been sustained at β_N $H_{89} > 9$ for 2 s or 16 energy confinement times. The heat transport in the advanced tokamak mode is similar to that in the high I_p conventional mode despite the higher q (necessary for obtaining a high f_{bs}) owing to a reduction in the turbulent transport from a combination of $E{\times}B$ shear, thermal ion dilution by fast beam ions, and $T_i > T_e$. The normalized beta achieved has exceeded the ideal no-wall stability limit by $\approx 15\%$, where it is limited by RWMs. Proof of principle experiments on RWM stabilization have modestly extended the high performance duration. Future experiments in DIII–D will use off-axis ECCD to eliminate the remaining inductive current to allow the study of stationary, fully non-inductive plasmas in the advanced operating mode.

REFERENCES

[1]   JT-60U TEAM, presented by Kikuchi M (1995) *Plasma Phys. Contr. Nucl. Fusion Research* (Proc. 15th Int. Conf., Seville, 1994) Vol. 1 (International Atomic Energy Agency, Vienna) p 31.

[2]   JET TEAM, presented by Watkins M L (1999) *Nucl. Fusion* **39**, 1227.

[3]   GREENE G J and HEDEMANN M A (1978) *Proc. Small Toroidal Plasma Devices Users Meeting* (DOE Report DOE-ET-78-G-05-5918).

[4]   ITER Physics Basis Editors *et al.* (1999) *Nucl. Fusion* **39**, 2137.

[5]   HIRSHMAN S P (1988) *Phys. Fluids* **31**,3150.

[6]   YUSHMANOV P N *et al.* (1990) *Nucl. Fusion* **30**,1999.

[7]   RICE B W *et al.* (1999) *Nucl. Fusion* **39**, 1855.

[8]   STRAIT E J (1997) *Phys. Plasmas* **4**,1783.

[9]   LA HAYE R J *et al.* (1997) *Nucl. Fusion* **37**, 397.

[10]   GÜNTER S *et al.* (1999) *Plasma Phys. Control. Fusion* **41**, 767.

[11]   LA HAYE R J *et al.* (1999) *Proc. 26th Eur. Conf. on Controlled Fusion and Plasma Physics, Maastricht, The Netherlands,* Vol 23J (European Physical Society, Petit-Lancy) p 1209.

[12]   DIII–D TEAM, presented by Taylor T S (1999) *Fusion Energy* (Proc. 17th Int. Conf., Yokohama, Japan,1998)} Vol 1 (International Atomic Energy Agency, Vienna) p 49.

[13]   GREENFIELD C M *et al.* (2000) *Phys. Plasmas* **7**, 1959.

[14]   GOLDSTON R *et al.* (1981) *J. Comput. Phys.* **43**, 61.

[15]   CHANG C S and HINTON F L (1986) *Phys. Fluids* **29**, 3314.

[16]   WALTZ R E *et al.* (1997) *Phys. Plasmas* **4**, 2482.

[17]   KONINGS J A and WALTZ R E (1997) *Nucl. Fusion* **37**, 863.

[18]   TANG W M *et al.* (1986) *Phys. Fluids* **29**, 3715.

[19]   DOMINGUEZ R R and WALTZ R E (1988) *Phys. Fluids* **31**, 3147.

[20]   WALTZ R E *et al.* (1998) *Phys. Plasmas* **5**, 1784.

[21]   WALTZ R E *et al.* (1994) *Phys. Plasmas* **1**, 2229.

[22]   STAEBLER G M *et al.* (1997) *Proc. 24th Euro. Conf. on Contr. Fusion and Plasma Phys., Berchtesgaden, Germany,* Vol 21A (European Physical Society, Petit-Lancy) Part III, p 1097.

[23]   PETTY C C *et al.* (1999) *Phys. Rev. Lett.* **83**, 3661.

[24]   LAO L L (2000) *Plasma Phys. Contr. Fusion* **42**, A51.

[25]   MCKEE G R *et al.* (2000) *Phys. Rev. Lett.* **84**,1922.

[26]   MCKEE G R *et al.* (2000) *Phys. Plasmas* **7**, 1870.

[27]   GAROFALO A M *et al.* (2000) *Nucl. Fusion*, to be published.

[28]   GAROFALO A M *et al.* (1999) *Phys. Rev. Lett.* **82**, 3811.

[29]   OKABAYASHI M *et al.* (1999) *Proc. 26th Eur. Conf. on Contr. Fusion and Plasma Phys., Maastricht, The Netherlands,* Vol 23J (European Physical Society, Petit-Lancy) p 1661.

[30]   RICE B W *et al.* (1996) *Plasma Phys. Contr. Fusion* **38**, 869.

[31]   FOREST C B *et al.* (1994) *Phys. Rev. Lett.* **73**, 2444.

[32]   LUCE T C *et al.* (1999) *Phys. Rev. Lett.* **83**, 4550.

[33]   LUCE T C *et al.* (1999) *Plasma Phys. Contr. Fusion* **41**, B119.

[34]   RICE B W *et al.* (1997) *Phys. Rev. Lett.* **79**, 2694.

[35]   PETTY C C *et al.* (2000) "Localized measurements of electron cyclotron current drive using MSE spectroscopy on the DIII–D tokamak," submitted to *Nucl. Fusion*.

ACKNOWLEDGMENT